Radiation Force Imaging: Challenges and Opportunities

Gregg E. Trahey, Mark Palmeri, Kathryn Nightingale, and Jeremy Dahl

Duke University
Durham, NC 27708
gregg.trahey@duke.edu

ABSTRACT

A number of novel imaging modalities have been developed to interrogate the mechanical properties of tissue. A subset of these methods utilize acoustic radiation force to mechanically excite tissue and form images from the local responses of tissue to these excitations. These methods are attractive because of the ability to focus and steer the excitatory beams and to control their spatial and temporal characteristics using techniques similar to those employed in conventional ultrasonic imaging. These capabilities allow for a wide variety of imaging methods whose features are only beginning to be explored. However, radiation force based methods also present significant challenges. Tissue and transducer heating limit the tissue displacements achievable with radiation force applications and restrict image frame rates and fields-of-view. The small tissue displacements are difficult to detect and may be obscured by physiologic tissue motion. We review the fundamental limits of imaging methods based on radiation force generated by patient safety concerns and the impact of these limits on achievable image signal-to-noise ratios and frame rates. We also review our progress to date in the development and clinical evaluation of one class of radiation force imaging methods employing very brief impulses of radiation force.

1. INTRODUCTION

Manual palpation of tissues for the purpose of disease identification and diagnosis has been employed for over 200 years, and is regularly performed by clinicians today. The utility of manual palpation is limited to more superficial and/or larger structures, as deeper and smaller structures are generally obscured by overlying tissues. Clinically palpable lesions are typically 1 cm in diameter or larger; lesions that are smaller than 1 cm or that lie deep within the organ of interest are typically not palpable. These clinically non-palpable lesions are usually easily palpable by pathologists after excision.

The goal of developing an imaging system capable of evaluating the mechanical properties of tissues at depth and with high resolution is being pursued by several researchers.[1–13] Methods for imaging the mechanical properties of tissues involve mechanical excitation of the tissue, and observation of the tissue response. The traditional types of excitation are static compression (i.e. elastography and strain-imaging,[3, 5, 12, 14] and quasi-static MRE[1]), and dynamic vibration excitation (i.e. sonoelasticity,[4, 15] and dynamic MRE[13, 16–18]). Traditionally, the source of the excitation has been external to the tissue, however, naturally occurring physiologic motion has also been utilized for arterial imaging[19] and for cardiac[20, 21] and arterial strain imaging.[11, 22]

Elastography (and strain imaging) has recently demonstrated some success in detecting and differentiating malignant from benign breast lesions,[23, 24] and in identifying organ transplant viability.[25]

Although acoustic radiation force is a phenomenon associated with the propagation of all acoustic waves, its effects are not generally apparent in diagnostic ultrasound. This is due to the relationship between the magnitude of the force and the intensity of the acoustic wave. In order to achieve appreciable displacements in tissue (ten microns) the intensity of the acoustic wave must be increased above that used for diagnostic imaging (*i.e.* 0.72 W/cm^2 [26]). Advances in transducer and system design in recent years have resulted in considerable increases in the maximum possible acoustic energy output from diagnostic ultrasound systems. This has sparked a renewed interest by several laboratories in the potential applications of acoustic radiation force.[7, 27–30] One application uses a radiation force field oscillating at the beat frequency of two confocal transducers to vibrate an object; the vibrations are detected by a hydrophone and used to generate an image.[31] In another application, acoustic radiation force is used to displace tissue, and the speed of the shear waves generated immediately after force removal is monitored to characterize variations in tissue Young's modulus.[7, 32, 33] In yet another application, acoustic radiation force is used to manipulate the vitreous humor of the eye.[27]

Many factors affect tissue response, including: tissue mechanical, acoustic, and geometric properties, and the magnitude and geometry of the applied radiation force. Application of acoustic radiation force gives rise to a region of excitation (ROE) within the tissue at a given time after radiation force excitation (∼0.1 ms). The ROE geometry is dictated by the attenuation (α), and speed of sound (c) of the tissue, and the focal characteristics and intensity (I) of the acoustic beam that generates the radiation force:[34]

$$F = \frac{2\alpha I}{c}. \tag{1}$$

Acoustic Radiation Force Impulse (ARFI) imaging is a radiation force based imaging method that uses acoustic pulses that are similar in frequency and amplitude to those used for focused ultrasound ablation procedures, however, they are of a much shorter duration (<1 ms, as compared to 1-5 seconds). The sequences used with ARFI imaging are designed to maintain thermal increases of less than 6°C, in order to avoid tissue damage.[35] In the following sections, we describe the challenges, limitations, and opportunities of radiation force imaging methods with specific examples given in relation to ARFI imaging.

2. METHODS

We have developed simulation tools, phantoms, and experimental systems to investigate the physics and imaging potential of various forms of radiation force imaging. Simulations performed with finite element models (FEM) and Field II,[36] and experiments in homogeneous phantoms were used to characterize the radiation force generated by a conventional linear array applying ARFI imaging pulses. The simulation methods used here are identical to that described in reference 37, and are briefly summarized here. Model meshes for FEM simulations were created in HyperMesh (Altair Computing Inc., Troy, MI) and imported into LS-DYNA3D (Livermore Software Technology Corporation, Livermore, CA) to solve the dynamic equations of motion for tissue displacement. Displacements determined in the FEM simulations were then used to model the displacement of scatterers in Field II. Image pulses created in Field II were then used to obtain rf signals before and after scatterer displacement.

We have implemented several radiation force imaging methods on Siemens SONOLINE Antares scanners (Siemens Medical Solutions USA, INC., Issaquah, WA). We are able to program pulse sequences on this scanner and control key features of the transmit and receive beamformer while acquiring raw radio-frequency data. These capabilities extend to a wide range of transducer arrays including those designed for cardiac, breast, abdominal and intracardiac imaging.

3. RESULTS AND DISCUSSION

3.1. Tissue displacement over time

Figure 1 shows simulation results which show tissue displacements at three time/distance scales as the tissue and is insonified by a 300-cycle 7.2 MHz pulse. The displacements correspond to those generated by a 128 element array focused at 20mm with a f-number (F/#) of 1.3. The tissue has an attenuation of 0.5 dB/cm-MHz, a Poisson's ratio of .499 and a Young's modulus of 1 kPa. The sinusoidal displacements in the first 45 μs correspond to the passage of the ultrasonic wave through the focal point. The roughly ± 0.4 micron displacements occur at the 7.2 MHz transmitted pulse frequency and are directly proportional to the transducer's source pressure and scaled by the tissue's acoustic velocity and density (1540 m/second and 1000 kg/m^3 in this simulation). During the first 5 microseconds of the pulse, a small (approximately 0.02 micron) net displacement resulting from radiation force can be observed in Figure 1(a). This displacement, in the direction of pulse propagation and away from the transducer, grows to approximately 2.6 micron at the end of the pulse (Figure 1(b)). After the passage of the pulse, sufficient momentum has been delivered to the tissue by the radiation force so that it continues to displace away from the transducer for approximately 0.4 ms and then recovers to its original position over the next 2 ms (Figure 1(c)). The magnitude of the radiation force-induced displacement depends on the energy in the applied pulse, its spatial and temporal characteristics, and on the tissue's acoustic attenuation, stiffness (Young's modulus), mass, and viscosity. The recovery time of the tissue depends largely on the shear modulus of the tissue.[7, 38]
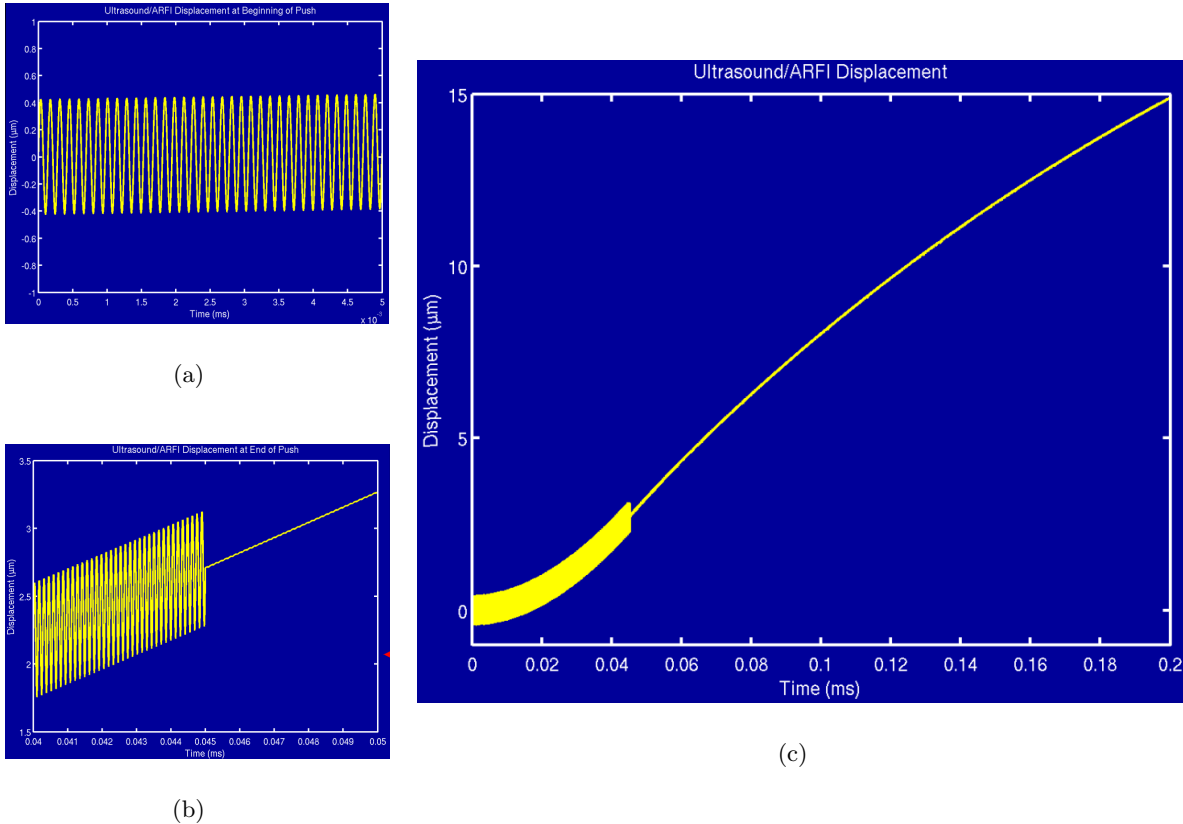
Figure 1. Axial particle displacements calculated for a 1 kPa tissue sample during insonification by a 7.2 MHz, 300 cycle pulse for (a) the first 5 μs of the pulse, (b) 50 μs during and after the pulse, and (c) 0.2 ms during and after the pulse. Over the following 2–3 ms, the particles return to their original positions.

The radiation force-induced tissue displacement is scaled by the pulse energy. The pulse pressure used to generate the results in Figure 1 is similar to those used in conventional B-mode and color Doppler applications, but the "pushing" pulse utilized is 100–200 times longer than conventional diagnostic pulses. We can scale the roughly 20 micron displacement in Figure 1 down by a factor of 100 to predict the radiation force induced displacement for a diagnostic pulse and further scale the displacement for a "typical" soft tissue Young's modulus of 10 kPa, yielding an expected displacement of .02 microns. Thus the expected radiation force induced tissue displacement from a single diagnostic pulse is small, even compared to the displacement induced by the passing acoustical pulse. Note that for an M-mode, color Doppler or spectral Doppler sequence, which would fire many pulses down one line of sight in rapid succession, the radiation force induced tissue momentum would accumulate over each pulse and could result in displacements many times larger than the 0.02 microns expected for a single pulse.

Figure 2 shows the experimentally acquired displacement patterns using transmit beam parameters similar to those employed in the simulation study results of Figure 1 applied to normal phantom materials with Young's moduli of 16 kPa and 4 kPa. The results are similar to those predicted by Figure 1 with appropriate scaling for the increased Young's moduli. A decrease in displacement is seen with increased Young's modulus. In addition, figure 2 displays other mechanical properties that can be measured from the tissue. These include the time to reach peak displacement (TTP) and the time required for the tissue to recover to within some distance of its original location (RT).
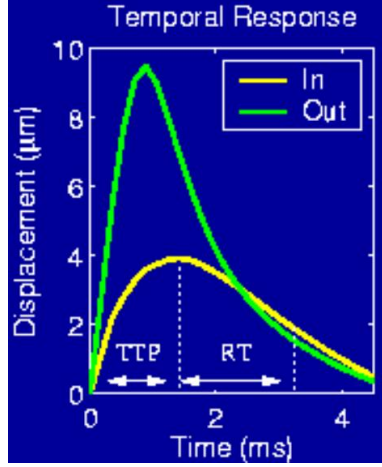
Figure 2. The tissue response to acoustic radiation force measured at the center of the region of excitation. The simulated tissue in this figure was a spherical inclusion with a Young's modulus of 16 kPa surrounded by a soft tissue region of 4 kPa. The line labeled "In" corresponds to the tissue response measured inside the spherical inclusion, and "Out" corresponds to the tissue response in the surrounding tissue.

3.2. Tissue displacement over space

Figure 3 shows the spatial pattern of radiation force induced tissue displacement 0.05 ms after the end of the applied "pushing" pulse. The transmitting array is at the top of the figures and corresponds to the array described in Figure 1. The displacement pattern roughly corresponds to the pulse intensity pattern generated in tissue for the selected array focal characteristics and tissue attenuation. However, the displacement pattern evolves over time as shear waves propagate from regions of insonification to lateral tissue structures. Figure 4 shows the evolution of tissue displacement over time, as shear waves propagate laterally and tissues in the region of excitation recover. Shear wave propagation speeds in tissue are expected to be in the 1–3 m/sec range, roughly three orders of magnitude slower than longitudinal wave propagation.

3.3. Detection of tissue displacements.

Most proposed radiation force imaging methods utilize correlation or Doppler methods to track the subtle tissue displacements expected to be generated. Walker and Trahey[39] have described the Cramer-Rao limits on tracking accuracy for such methods.

Equation 2 shows the expected jitter for an unbiased estimator tracking tissue displacements,

$$\sigma_{RF}(\Delta x - \Delta \hat{x}) \geq \frac{c}{2} \sqrt{\frac{2N_0}{A^2 \sqrt{\pi} \left(4\pi^2 f_0^2 \sigma_t + \frac{1}{2\sigma_t}\left(1 - e^{-4\pi^2 f_0^2 \sigma_t^2}\right)\right)}} \tag{2}$$

where f_0 is the center frequency in Hertz, A is a scaling factor in volts, σ_t is a constant defining the pulse length (inversely proportional to bandwidth) given in seconds, c is the speed of sound in meters per second, and N_0 is the noise power spectral height in units of $(Volts)^2$ seconds. McAleavey et al.[40] has analyzed the relevant noise sources in tracking tissues displaced by radiation force. He describes the bias and jitter introduced by the shearing of tissues, as visible in Figure 3. Under typical imaging conditions, the expected jitter associated in tissue tracking tasks is in the 0.2–0.4 micron range. Given the 5–20 micron displacements anticipated for imaging conditions reflected in the results in Figures 1–3, reasonable signal-to-noise ratios are expected and have been achieved[8, 29, 41] in radiation force imaging. However the tissue displacements induced by radiation force from normally operating diagnostic ultrasonic scanners is likely near or below detectable levels if conventional detection methods are employed.
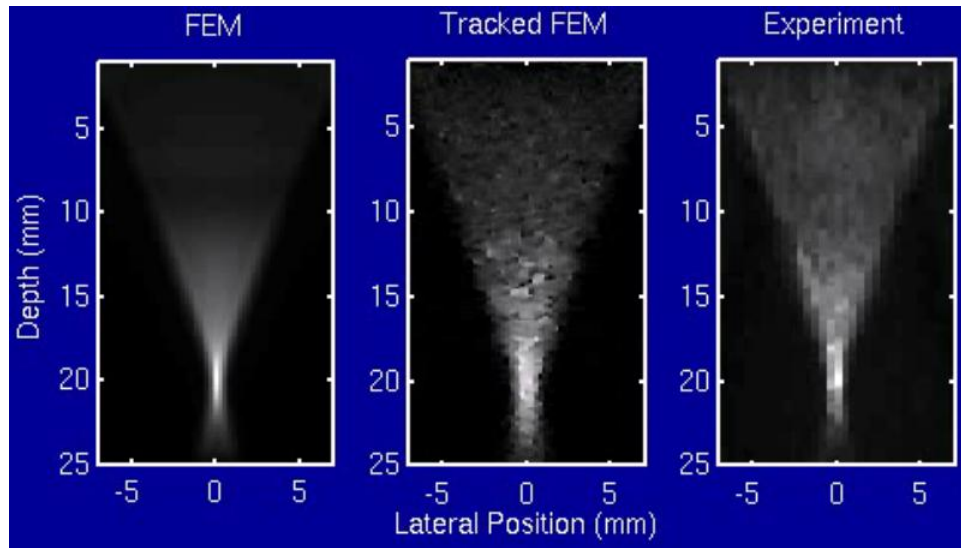
Figure 3. Displacement induced by radiation force for a conventional linear array, 1 ms after application of the radiation force. On the left is the displacement predicted by a finite element simulation. In the middle is the predicted displacement from the finite element model is measured using ultrasonic methods. On the right is the estimated displacement using ultrasonic tracking methods of an experimentally applied radiation force to a tissue-mimicking phantom from a conventional linear array. Jitter is apparent in the images showing the displacements measured with ultrasonic tracking methods.
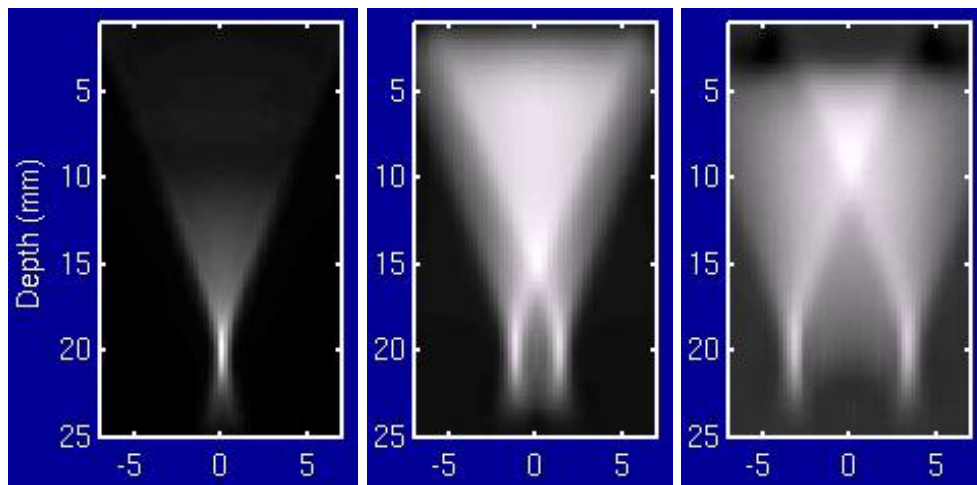

Figure 4. A finite element simulation of the propagation of shear waves resulting from radiation force. The transducer is located at the top of the images. On the left is the radiation force-induced displacements 0.1 ms after application of the force. The middle and right images show the displacements 1.2 ms and 2.4 ms, respectively, after application of the force. The shear waves propagate out of the imaging plane as well.

3.4. Tissue heating

We have conducted extensive experimental and simulation studies of the tissue heating caused by ultrasonic pulses with sufficient energy to induce measurable tissue displacements.[41,42] The spatial patterns of heat deposition match those of tissue displacement before shear wave propagation has occurred (Figure 3). The heat propagates and dissipates much more slowly than the displacement patterns and is largely effected by local blood perfusion rates.[41] The temperature increase associated with the conditions described in Figure 1 is 0.2°C. Peak heating will occur at the termination of the acoustical pulse, well before peak tissue displacement occurs.
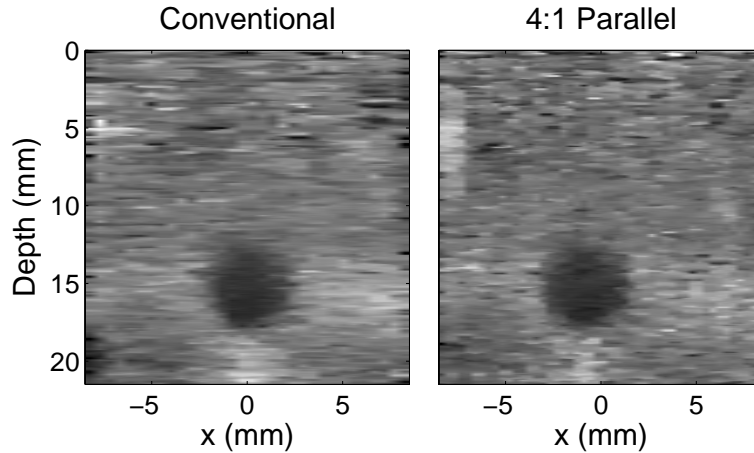
Figure 5. An ARFI image generated by conventional tracking is compared with that generated by parallel tracking. For this image, conventional tracking (ratio of 1 track location to 1 push beam) uses 0.53 mm spacing between push (and track) locations. 4:1 parallel tracking (4 track locations to 1 push beam) uses 1.42 mm spacing between push locations and 0.35 mm spacing between tracked locations. To generate the image on the left, 32 applications of radiation force were required. For the right image, only 12 applications were required. Note that the conventional image can be generated using 0.35 mm spacing as well, which will improve the spatial resolution, but at the cost of additional heating due to more applications (48 required) of radiation force. These images were created 0.72 ms after application of radiation force.

A rough rule of thumb provided by the results associated with Figures 1 and 2 for a 10 kPa tissue is that a temperature increase of 0.2°C is associated with a 0.8 micron displacement induced by radiation force. Given a 0.2 micron noise floor, the SNR for this experimental condition would be 40, sufficient to yield very high quality images.

The 0.2°C temperature increase described above is well within thermal safety limits described by the FDA in the context of ultrasonic imaging.[26] However, repeated applications of "pushing pulses" will cause a gradual increase in temperatures that could easily exceed thermal safety limits.[42] Thus, it is important to increase the tissue information obtained with each pushing pulse.

One method by which to increase the efficiency of the radiation force method is to employ parallel-receive beamforming.[43, 44] In reference 44, parallel-receive beamforming was used to concurrently track the displacements at multiple locations. This allowed for fewer applications of radiation force in order to produce the desired effect, in this case generation of displacement images. Because there are fewer applications of radiation force, the temperature increase in the patient and the temperature increase of the transducer are both reduced.

Figure 5 shows an example of the benefit of parallel tracking in ARFI imaging. In the image on the left, a displacement image is shown of a hard spherical inclusion (31 kPa) surrounded by a soft region (4 kPa), generated from conventional tracking methods where the ratio between the number of applications of radiation force and the number of ultrasonically tracked locations is 1. For this image, 32 applications of radiation force were required to create the image. For the image on the right in figure 5, an identical displacement image is created using 4:1 parallel tracking methods where there are 4 tracked locations for every application of radiation force. To create this image, only 12 applications of radiation force were required. This implies that less heat will be generated per frame of ARFI imaging.

Using the same sample spacing from figure 5, we computed the expected increase in temperature for an ARFI image using 72 applications of radiation force for conventional tracking methods. The peak increase in tissue heating for a single frame reaches 0.1°C, and 0.45°C for 5 consecutive frames at a rate of 2.8 frames per second (fps). To image the same field-of-view, the 4:1 parallel tracking method requires only 27 applications of radiation force. This yields an increase of 0.1°C for a single frame, the same as in the conventional case, however an increase of only 0.18°C was observed in 5 consecutive frames at 2.8 fps.

In addition, we experimentally measured the transducer surface heating for a VF7-3 (Siemens Medical Solutions USA, Inc, Issaquah, WA) linear array for the above conventional and parallel tracking methods. For conventional tracking, a single displacement image incurred an increase in surface temperature of 0.37°C, and five consecutive images at 2.8 fps generated a temperature increase of 1.7°C. For parallel tracking, a single displacement image incurred a 0.17°C increase in surface temperature, and five consecutive images at 2.8 fps caused a 0.63°C increase in surface temperature. Smaller temperature increases in the parallel tracking methods are a direct result of fewer applications of radiation force.

4. CONCLUSIONS

Radiation force based imaging methods are capable of measuring the mechanical properties of tissue. We have described current limitations and challenges for ultrasonic based tracking methods of the tissue response to the radiation force. These limitations include a fundamental limit on the noise of the estimates of the tissue displacements generated by the radiation force, patient heating due to absorption of the radiation force by the tissue, and surface heating of the transducer. Limitations due to noise in the estimates are fairly easy overcome, while limitations due to heating still remain a challenge. New improvements, such as parallel tracking methods, have been employed to improve the heating characteristics of the patient and the transducer, and show promise for bringing ultrasonic-based, radiation force imaging methods to market.

ACKNOWLEDGMENTS

REFERENCES

1. D. Plewes, J. Bishop, A. Samani, and J. Sciarretta, "Visualization and quantification of breast cancer biomechanical properties with magnetic resonance elastography," *Phys. Med. Biol.* **45**(1), pp. 1591–1610, 2000.

2. R. Muthupillai, D. Lomas, P. Rossman, J. Greenleaf, A. Munduca, and R. Ehman, "Magnetic resonance elastography by direct visualization of propagating acoustic strain waves," *Science* **269**, pp. 1854–1857, 1995.

3. J. Ophir, S. Alam, B. Garra, F. Kallel, E. Konofagou, T. Krouskop, and T. Varghese, "Elastography: ultrasonic estimation and imaging of the elastic properties of tissue," *Proc. Inst. Mech. Engrs* **213**, pp. 203–233, 1999.

4. L. Taylor, B. Porter, D. Rubens, and K. Parker, "Three-dimensional sonoelastography: Principles and practices," *Phys. in Med. Biol.* **45**, pp. 1477–1494, 2000.

5. T. Hall, Y. Zhu, J. Jaing, and L. Cook, "Noise reduction strategies in freehand elasticity imaging," in *Proceedings of the 2002 IEEE Ultrasonics Symposium*, 2002.

6. Y. Zhu, P. Chaturvedi, and M. Insana, "Strain imaging with a deformable mesh," *Ultrasonic Imaging* **21**(2), pp. 127–146, 1999.

7. A. Sarvazyan, O. Rudenko, S. Swanson, J. Fowlkes, and S. Emelianov, "Shear wave elasticity imaging: A new ultrasonic technology of medical diagnostics," *Ultrasound Med. Biol.* **24**(9), pp. 1419–1435, 1998.

8. K. Nightingale, M. Soo, R. Nightingale, and G. Trahey, "Acoustic radiation force impulse imaging: In vivo demonstration of clinical feasibility," *Ultrasound Med. Biol.* **28**(2), pp. 227–235, 2002.

9. W. Walker, F. Fernandez, and L. Negron, "A method of imaging viscoelastic parameters with acoustic radiation force," *Phys. Med. Bio.* **45**(6), pp. 1437–1447, 2000.

10. L. Sandrin, M. Tanter, S. Catheline, and M. Fink, "Shear modulus imaging with 2-d transient elastography," *IEEE Trans. Ultrason., Ferroelec., Freq. Contr.* **49**(4), pp. 426–435, 2002.

11. C. de Korte and A. van der Steen, "Intravascular ultrasound elastography: an overview," *Ultrasonics* **40**, pp. 859–865, 2002.

12. D. Steele, T. Chenevert, A. Skovoroda, and S. Emelianov, "Three-dimensional static displacement, stimulated echo NMR elasticity imaging," *Phys. Med. Biol.* **45**(1), pp. 1633–1648, 2000.

13. A. McKnight, J. Kugel, P. Rossman, A. Manduca, L. Hartmann, and R. Ehman, "MR elastography of breast cancer: Preliminary results," *AJR* **178**(6), pp. 1411–1417, 2002.

14. M. Bilgen and M. Insana, "Elastostatics of a spherical inclusion in homogeneous biological media," *Physics in Medicine and Biology* **43**(1), pp. 1–20, 1998.

15. D. Fu, S. Levinson, S. Gracewski, and K. Parker, "Noninvasive quantitative reconstruction of tissue elasticity using an interative forward approach," *Phys. Med. Biol.* **45**(6), pp. 1495–1509, 2000.

16. E. Van Houten, J. Weaver, M. Miga, F. Kennedy, and K. Paulsen, "Elasticity reconstruction from experimental MR displacement data: initial experience with an overlapping subzone finite element inversion process," *Medical Physics* **27**(1), pp. 101–107, 2000.

17. T. Oliphant, A. Manduca, R. Ehman, and J. Greenleaf, "Complex-valued stiffness reconstruction fro magnetic resonance elastography by algebraic inversion of the differential equation," *Magnetic Resonance in Medicine* **45**, pp. 299–310, 2001.

18. R. Sinkus, J. Lorenzen, D. Schrader, M. Lorenzen, M. Dargatz, and D. Holz, "High-resolution tensor MR elastography for breast tumour detection," *Phys. Med. Biol.* **45**(6), pp. 1649–1664, 2000.

19. D. K. Arnett, G. W. Evans, and W. Riley, "Arterial stiffness: a new cardiovascular risk factor?," *Am. J. Epidemiology* **140**, pp. 669–682, 1994.

20. J. D'hooge, B. Bijnens, J. Thoen, and et. al., "Echocardiographic strain and strain-rate imaging: A new tool to study regional myocardial function," *IEEE Transactions on Medical Imaging* **21**(9), pp. 1022–30, 2002.

21. T. Varghese, J. Zagzebski, P. Rahko, and et. al., "Ultrasonic imaging of myocardial strain using cardiac elastography," *Ultrasonic Imaging* **25**(1), pp. 1–16, 2003.

22. J. Mai, J. K. Tsou, C. Pellot-Barakat, W. Hornof, C. Kargel, and M. Inasana, "Vascular compliance using elasticity imaging," in *Proceedings of the 2001 Ultrasonics Symposium*, pp. 1577–1580, 2001.

23. B. Garra, E. Cespedes, J. Ophir, S. Spratt, R. Zuurbier, C. Magnant, and M. Pennanen, "Elastography of breast lesions: Initial clinical results," *Radiology* **202**, pp. 79–86, 1997.

24. T. Hall, Y. Zhu, and C. Spalding, "In vivo real-time freehand palpation imaging," *Ultrasound Med. Biol.* **29**(3), pp. 427–435, 2003.

25. S. Emelianov, M. Lubinski, A. Skovoroda, R. Erkamp, S. Leavey, R. Wiggins, and M. O'Donnell, "Reconstructive ultrasound elasticity imaging for renal transplant diagnosis: kidney ex vivo results," *Ultrasonic Imaging* **22**, pp. 178–194, July 2000.

26. Center for Devices and Radiological Health (CDRH), "510(k) guide for measuring and reporting acoustic output of diagnostic ultrasound medical devices," *U S Dept of Health and Human Services 1985, Rev. 1993,* , Dec. 1994.

27. W. Walker, "Internal deformation of a uniform elastic solid by acoustic radiation force," *J. Acoust. Soc. Am.* **105**(4), pp. 2508–2518, 1999.

28. T. Sugimoto, S. Ueha, and K. Itoh, "Tissue hardness measurement using the radiation force of focused ultrasound," in *Proceedings of the 1990 Ultrasonics Symposium*, pp. 1377–1380, 1990.

29. K. Nightingale, R. Nightingale, T. Hall, and G. Trahey, "The use of radiation force induced tissue displacements to image stiffness: a feasibility study." 23rd International Symposium on Ultrasonic Imaging and Tissue Characterization, May 27-29, 1998.

30. M. Fatemi and J. Greenleaf, "Ultrasound-stimulated vibro-acoustic spectrography," *Science* **280**, pp. 82–85, 1998.

31. M. Fatemi and J. Greenleaf, "Vibro-acoustography: An imaging modality based on utrasound-stimulated acoustic emission," *Proc. Natl. Acad. Sci.* **96**, pp. 6603–6608, 1999.

32. J. Bercoff, S. Chaffai, M. Tanter, and M. Fink, "Ultrafast imaging of beamformed shear waves induced by the acoustic radiation force in soft tissues: Application to transient elastography," in *Proceedings of the 2002 IEEE Ultrasonics Symposium*, 2002.

33. K. Nightingale, S. McAleavey, and G. Trahey, "Demonstration of shear wave generation using acoustic radiation force: in vivo and ex vivo results," *UMB* , in review.

34. W. Nyborg, "Acoustic streaming," in *Physical Acoustics*, W. Mason, ed., **IIB**, ch. 11, pp. 265–331, Academic Press Inc, New York, 1965.

35. M. Palmeri, G. Trahey, R. Nightingale, and K. Nightingale, "A finite element model of the heating generated during acoustic remote palpation," *IEEE Trans. Ultrason., Ferroelec., Freq. Contr.* , in review.

36. J. A. Jensen, "Field: A program for simulating ultrasound systems," *Med. Biol. Eng. Comp., col. 10th Nordic-Baltic Conference on Biomedical Imaging* **4**(1), pp. 351–353, 1996.

37. M. L. Palmeri, S. A. McAleavey, G. E. Trahey, and K. R. Nightingale, "Ultrasonic tracking of acoustic radiation force-induced displacements in homogeneous media," *IEEE Transactions on Ultrasonics, Ferroelectrics and Frequency Control* **53**(7), pp. 1300–1313, 2006.

38. M. L. Palmeri, S. A. McAleavey, K. L. Fong, G. E. Trahey, and K. R. Nightingale, "Dynamic mechanical response of elastic spherical inclusions to impulsive acoustic radiation force excitation," *IEEE Trans Ultrason Ferroelectr Freq Control* **53**, pp. 2065–2079, Nov 2006.

39. W. Walker and G. Trahey, "A fundamental limit on delay estimation using partially correlated speckle signals," *IEEE Trans. Ultrason., Ferroelec., Freq. Contr.* **42**(2), pp. 301–308, 1995.

40. S. McAleavey, K. Nightingale, and G. Trahey, "Estimates of echo correlation and measurement bias in acoustic radiation force impulse imaging," *IEEE Trans. Ultrason., Ferroelec., Freq. Contr.* **50**(6), pp. 631–641, 2003.

41. B. J. Fahey, K. R. Nightingale, R. C. Nelson, M. L. Palmeri, and G. E. Trahey, "Acoustic radiation force impulse imaging of the abdomen: demonstration of feasibility and utility," *Ultrasound Med Biol* **31**, pp. 1185–1198, Sep 2005.

42. M. Palmeri and K. Nightingale, "On the thermal effects associated with radiation force imaging of soft tissue," *IEEE Trans. Ultrason., Ferroelec., Freq. Contr.* **51**(5), pp. 551–565, 2004.

43. J. Bercoff, M. Tanter, and M. Fink, "Supersonic shear imaging: A new technique for soft tissue elasticity mapping," *IEEE Transactions on Ultrasonics, Ferroelectrics and Frequency Control* **51**(4), pp. 396–409, 2004.

44. J. J. Dahl, G. F. Pinton, M. L. Palmeri, V. Agrawal, K. R. Nightingale, and G. E. Trahey, "A parallel tracking method for acoustic radiation force impulse imaging," *IEEE Transactions on Ultrasonics, Ferroelectrics and Frequency Control* **54**(2), pp. 301–312, 2007.